ARKTALAS ASC-1: Characterize Arctic Amplification and its impact?

The Arctic amplification and its impact: Attribution through remote-sensing data

Co-authors (tentatively):

Igor Esau[1,2], Johnny Johannesen[1], Lasse Pettersson[1], Aleksander Chernokulsky[3], Oleg Sizov[4] and …

The Copernicus Sentinel-2 image of oil (diesel) spill into the river Ambarnaya near Norilsk, Russia. The image from June 1st, 2020, was processed by ESA and made available under CC BY-SA 3.0 IGO license on https://www.esa.int/ESA_Multimedia/Images/2020/06/Arctic_Circle_oil_spill.

Courtesy: Esau et al.

Figure 1

Emergence of the *apparent* Amplification

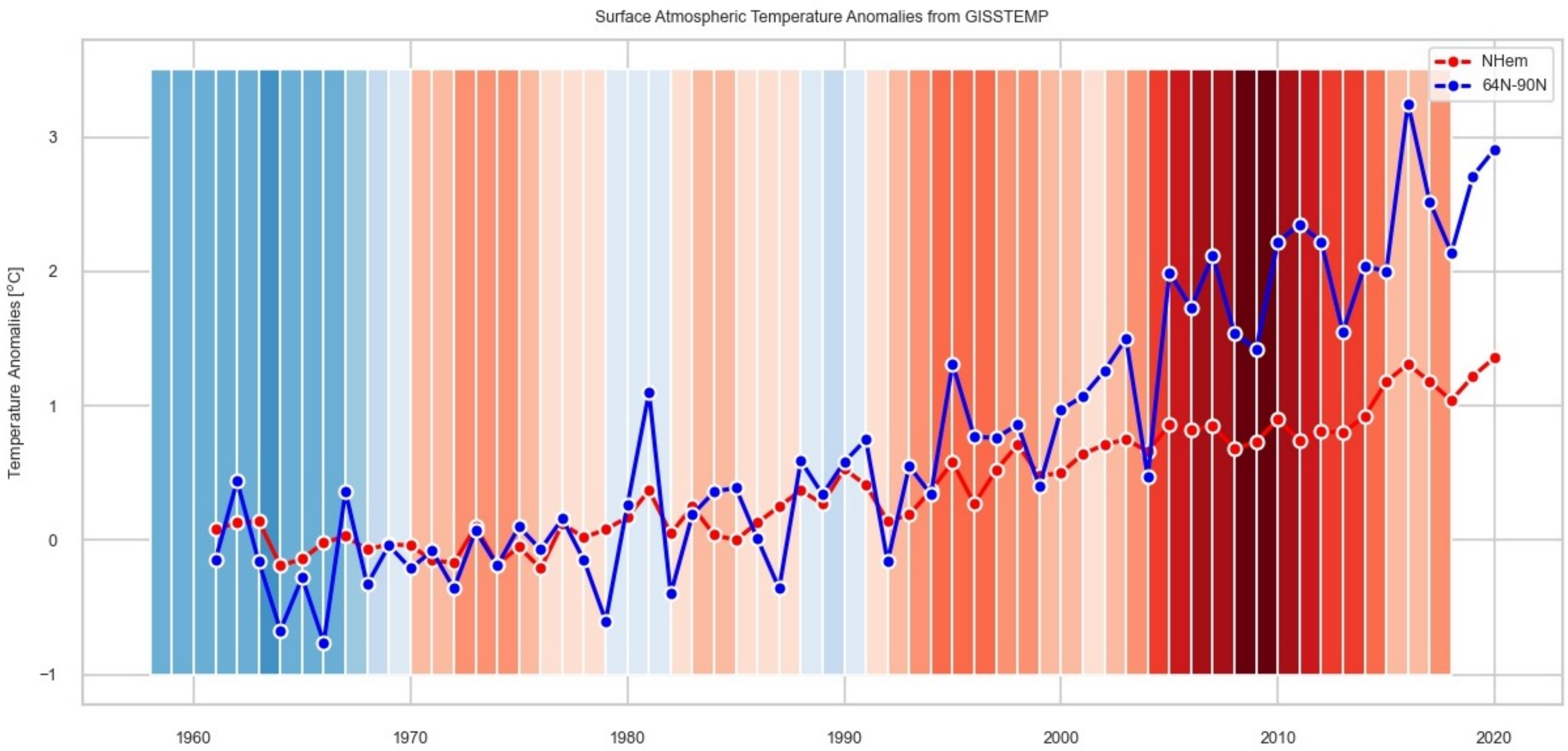

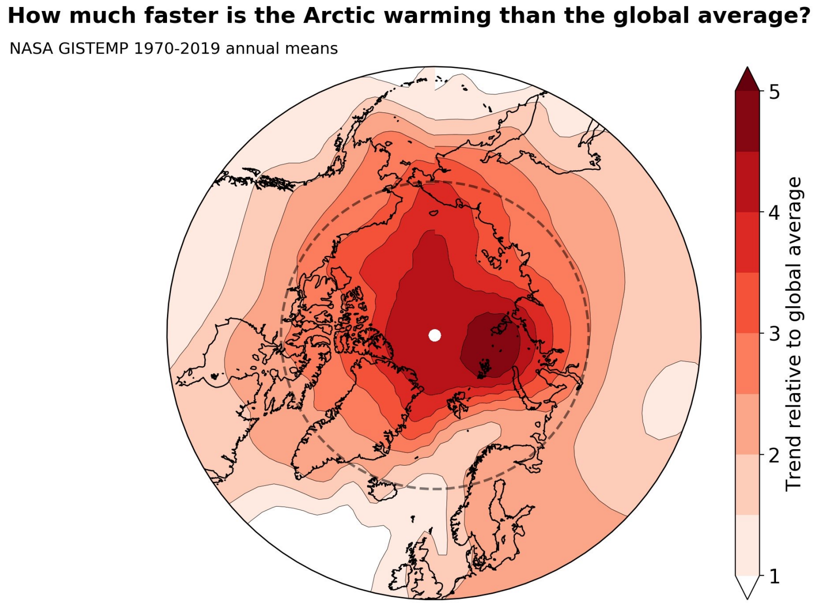

Emergence of the Arctic Amplification shown through the annual temperature anomalies in high latitudes (64N-90N, blue line) and the Northern Hemisphere (NHem, red line). The color strips show divergence rate of temperature anomalies averaged within 7-years moving window. Red – high divergence rate, blue – negative divergence (convergence) rate. Dataset: GISTEMP/AIRS.

Theory:

Alexeev, V.A., Langen, P.L., Bates, J.R., 2005. Polar amplification of surface warming on an aquaplanet in “ghost forcing” experiments without sea ice feedbacks. Clim. Dyn. 24, 655–666. https://doi.org/10.1007/s00382-005-0018-3

Alexeev, V.A., Jackson, C.H., 2013. Polar amplification: Is atmospheric heat transport important? Clim. Dyn. 41, 533–547. https://doi.org/10.1007/s00382-012-1601-z

$$H\, dT_1/dt = S_1 - F - (A + BT_1) + \varepsilon$$
$$H\, dT_2/dt = S_2(1 - 2\alpha a) + F - (A + BT_2) + \varepsilon$$

$$F = F_0 + \gamma_1(T_1 - T_2) + \gamma_2 C(T_1)(T_1 - T_2)$$

2 modes of solution:
- *Fast – corresponds to the Amplification*
- *Slow – corresponds to ocean responses*

- Climate processes are slow – require decades of observations
- Understanding of climate processes requires models – models are imperfect
- Climate processes are complex and interactive – require multiple observational datasets (products)

Reanalysis, models imperfections, and discrepancies

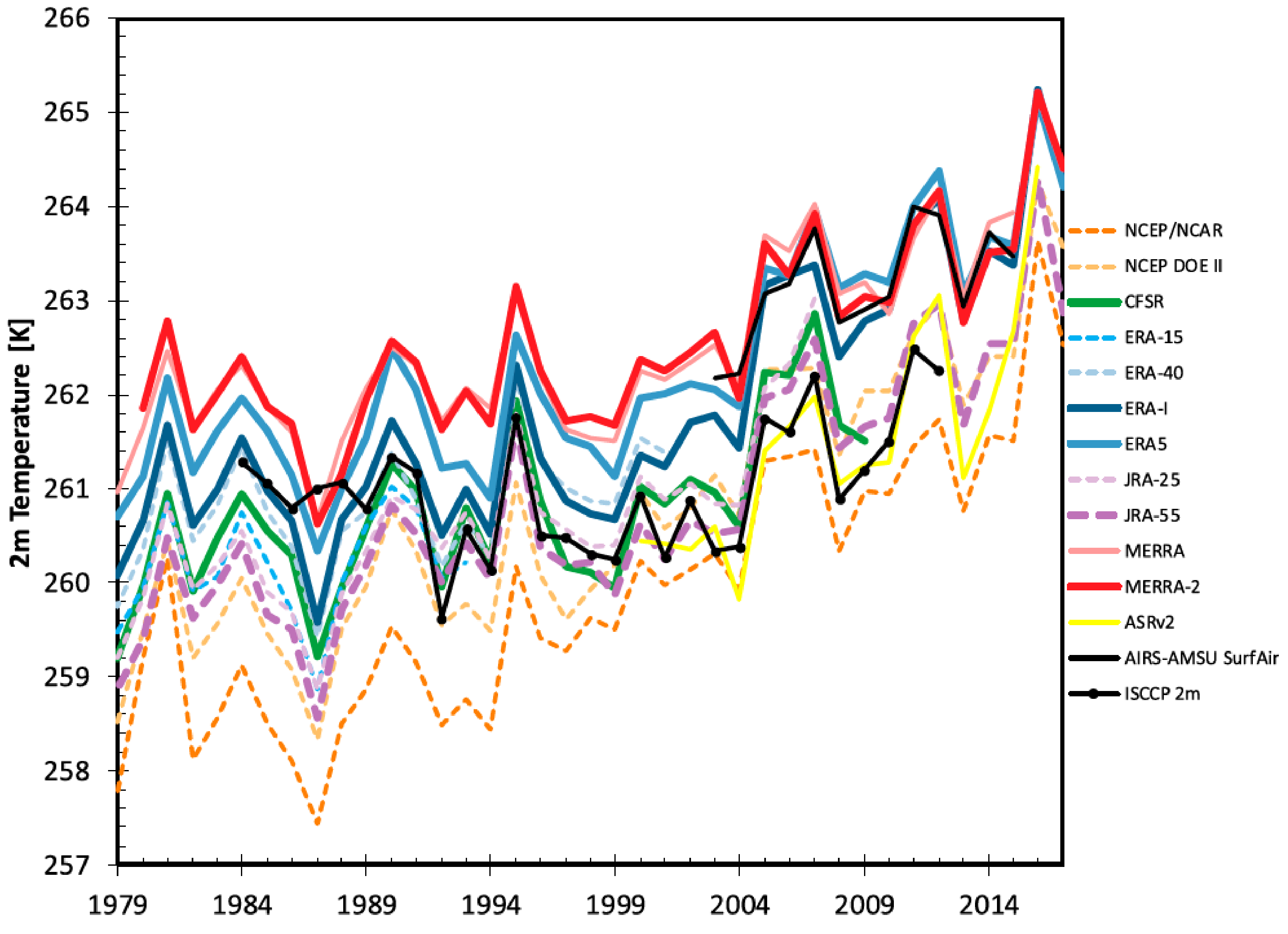

Time series of annual 2-m temperature averaged over Arctic Ocean domain from 12 reanalyses (K). Reanalyses using threshold ice cover are show as dashed lines, and five contemporary reanalyses are indicated with bold lines. Corresponding AIRS-AMSU and ISCCP 2-m air temperature are also shown.

Marquardt Collow, A.B., Cullather, R.I., Bosilovich, M.G., 2020. Recent arctic ocean surface air temperatures in atmospheric reanalyses and numerical simulations. J. Clim. 33, 4347–4367. https://doi.org/10.1175/JCLI-D-19-0703.1

Essential climate variables in ESA CCI

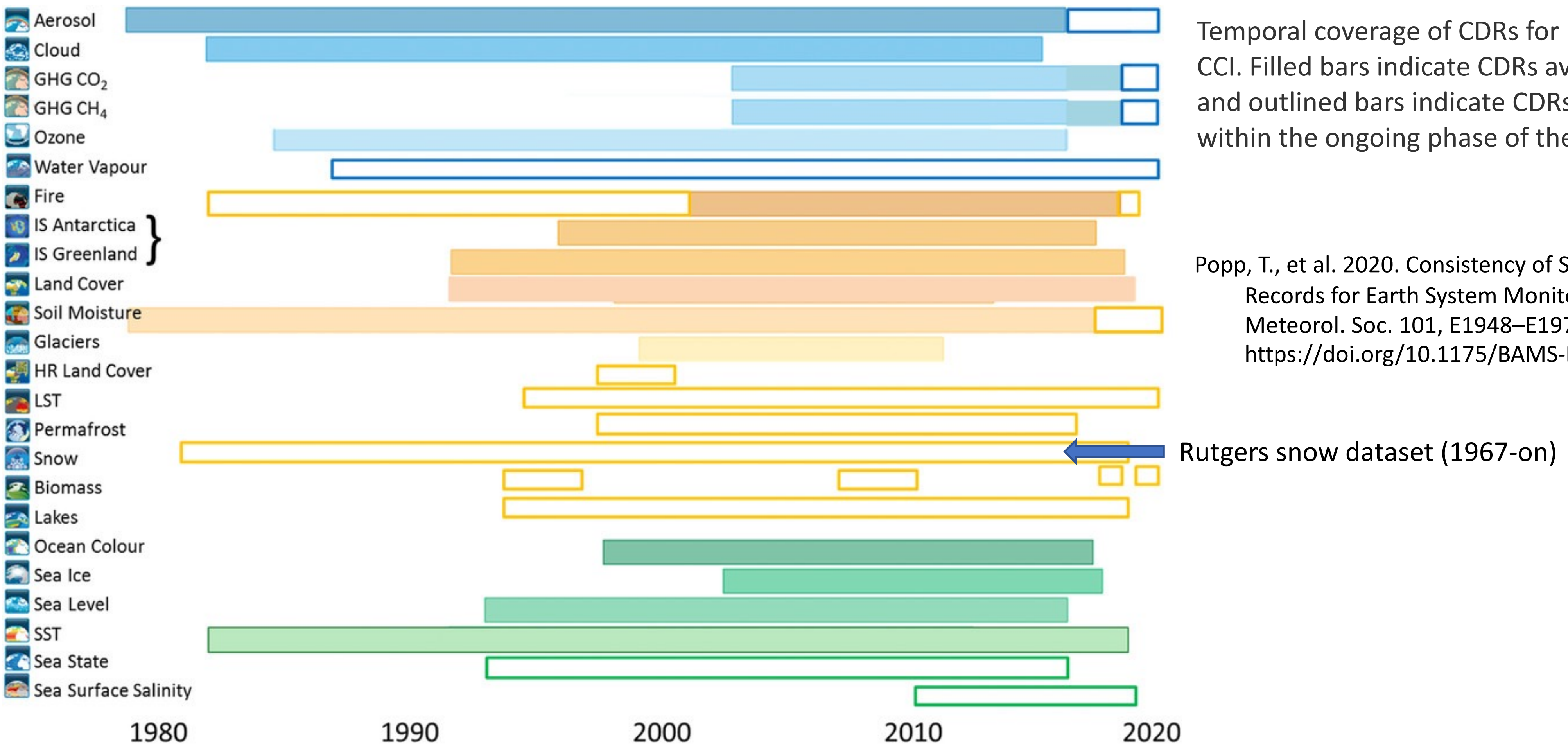

Temporal coverage of CDRs for ECVs analyzed by CCI. Filled bars indicate CDRs available in 2019, and outlined bars indicate CDRs that are planned within the ongoing phase of the CCI program.

Popp, T., et al. 2020. Consistency of Satellite Climate Data Records for Earth System Monitoring. Bull. Am. Meteorol. Soc. 101, E1948–E1971. https://doi.org/10.1175/BAMS-D-19-0127.1

Arctic Data Availability and Quality

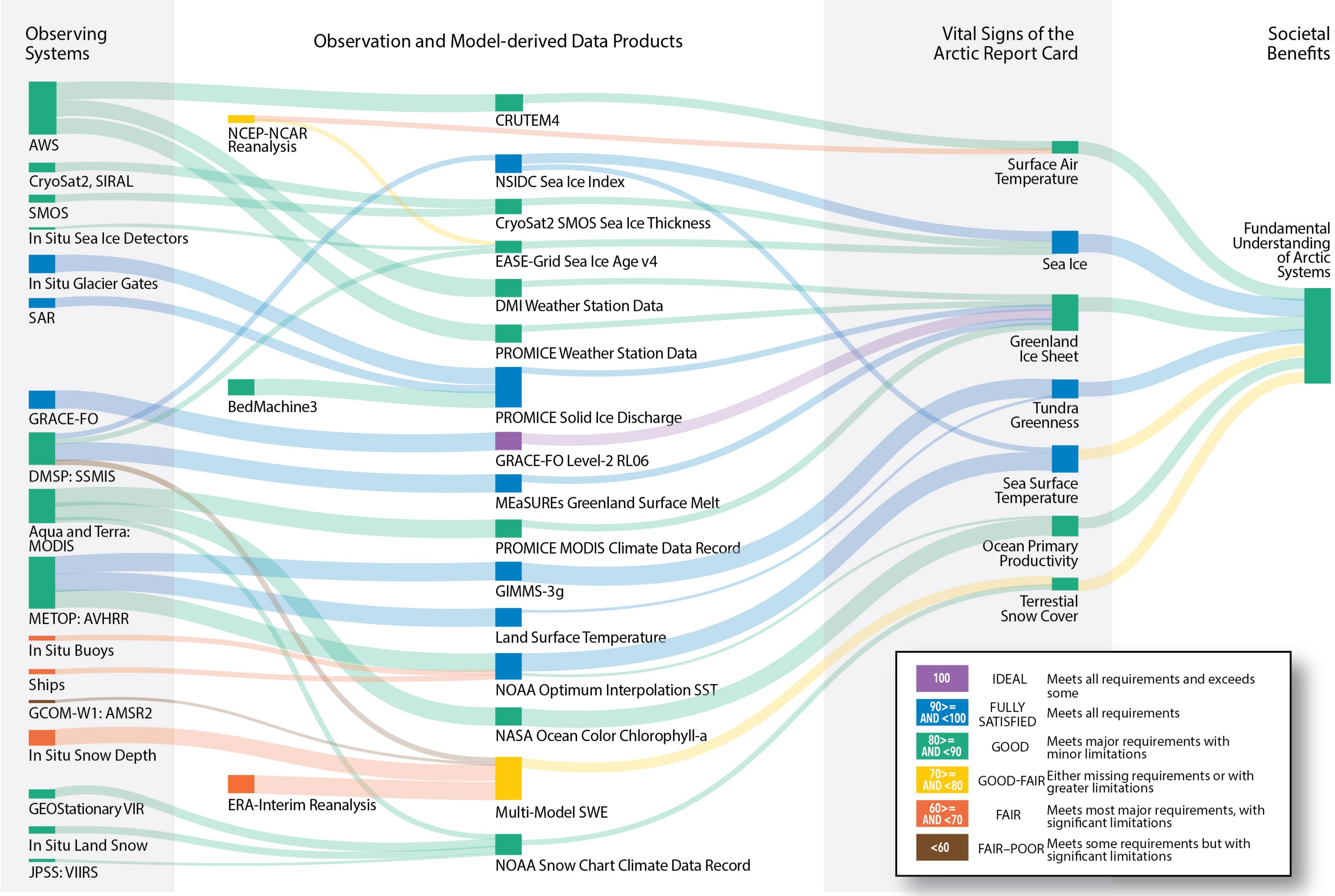

Source:

15-Year Retrospective Analysis on AON

The Observational Foundation of the Arctic Report Card - a 15-Year Retrospective Analysis on the Arctic Observing Network (AON) and Insights for the Future System *DOI: 10.25923/ahj5-z336*

by S. Starkweather, H. Shapiro, S. Vakhutinsky, and M. Druckenmiller

The Amplification: observations and models before 2000

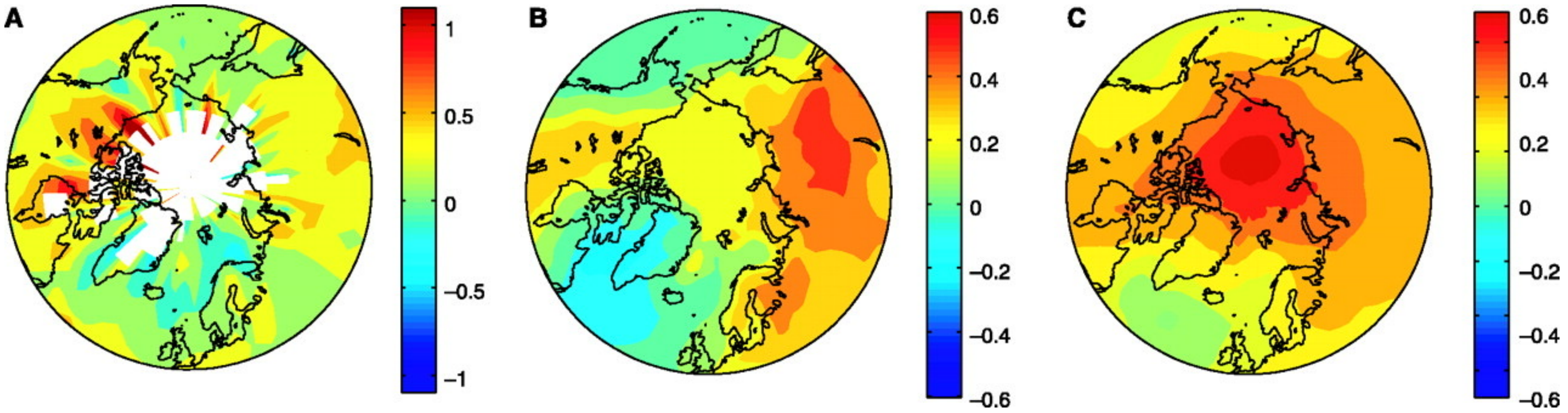

Late XXth century (before 2000) – major discrepancy between modelling results and observations

Trends in SAT (**A**) estimated **from observations**, for all months from 1971–2000. [Estimates were provided by W. Chapman] (**B**) SAT trends estimated from the National Centers for Environmental Prediction/National Center for Atmospheric Research (NCEP/NCAR) **reanalysis**, regressed on the AO index for all months from 1948–2002 and multiplied by the trend in the winter AO index. (**C**) SAT trends **simulated** as a response to doubling carbon dioxide levels, averaged over 19 models participating in the Coupled Model Intercomparison Project. The trend was calculated from the temperature difference averaged for all months in years 60 to 80 from simulations with a transient 1% increase per year in carbon dioxide minus the 80-year average from a control run with preindustrial carbon dioxide levels divided by 7 decades. Units in (A), (B), and (C) are °C per decade.

Moritz, R.E., Bitz, C.M., Steig, E.J., 2002. Dynamics of Recent Climate Change in the Arctic. Science (80-.). 297, 1497–1502. https://doi.org/10.1126/science.1076522

UAH MSU atmospheric temperature trends

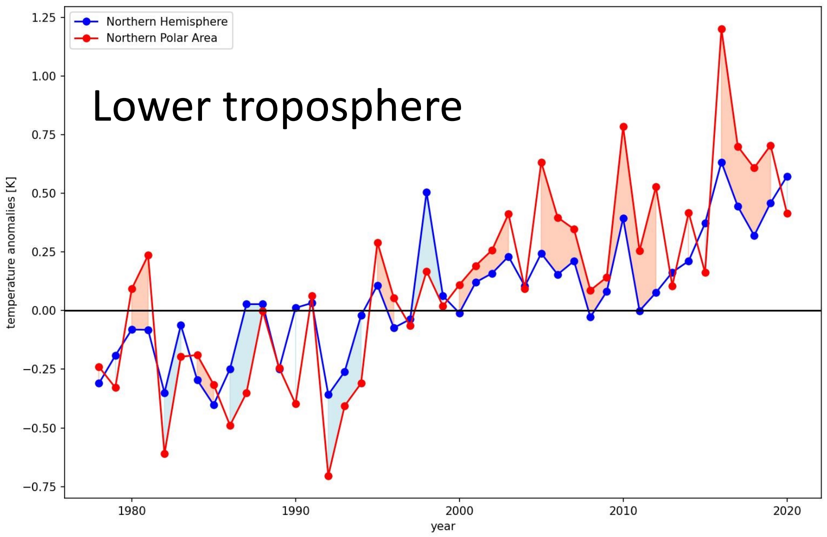

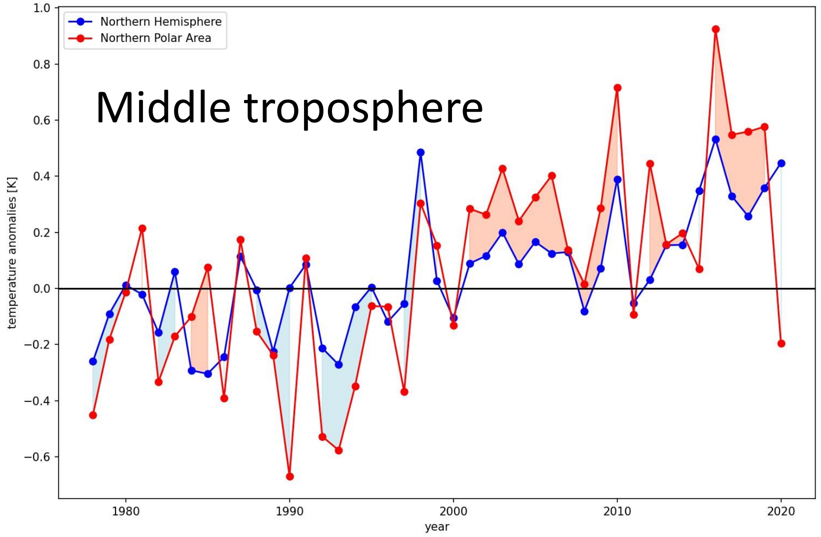

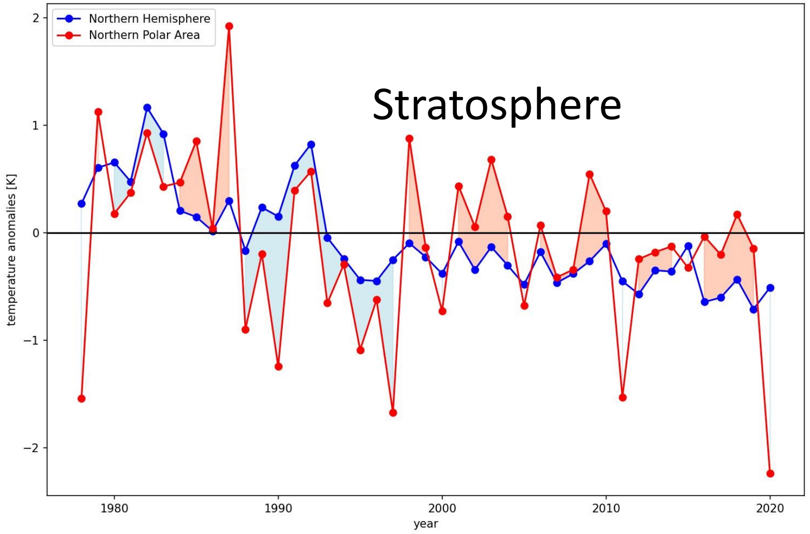

UAH MSU atmospheric temperature anomalies

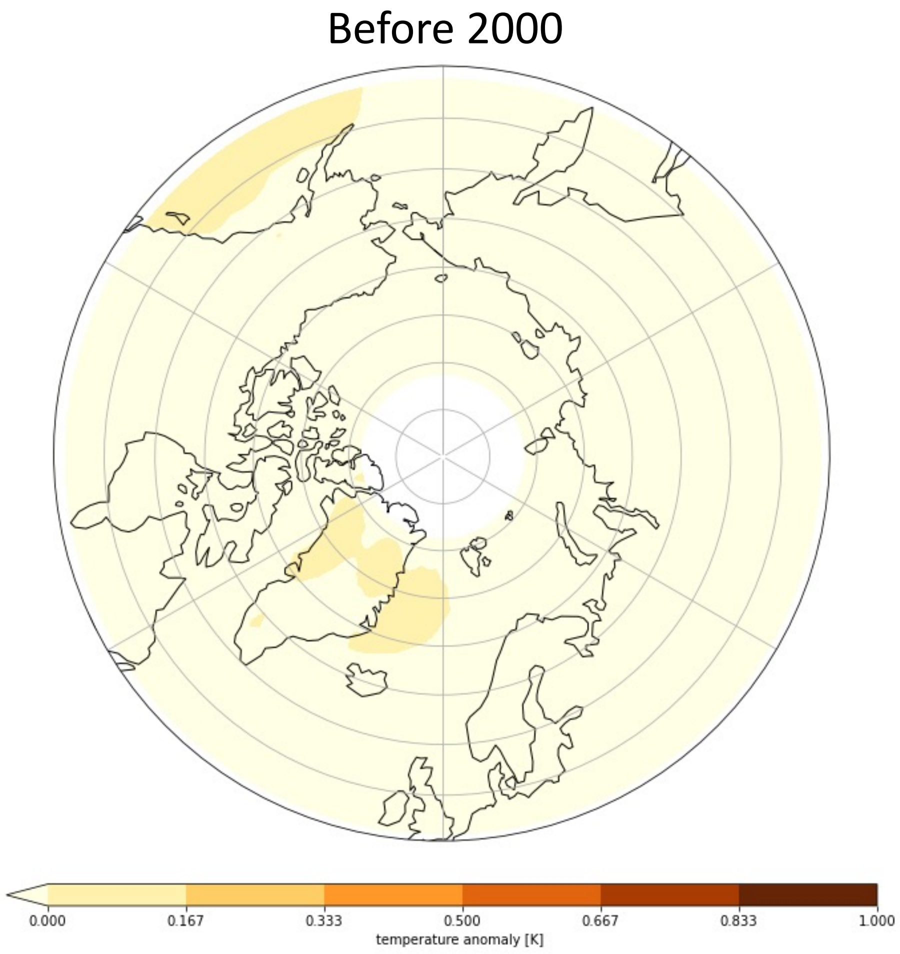

Lower troposphere
Annual anomalies

Emergence of the apparent Amplification (before 2000)

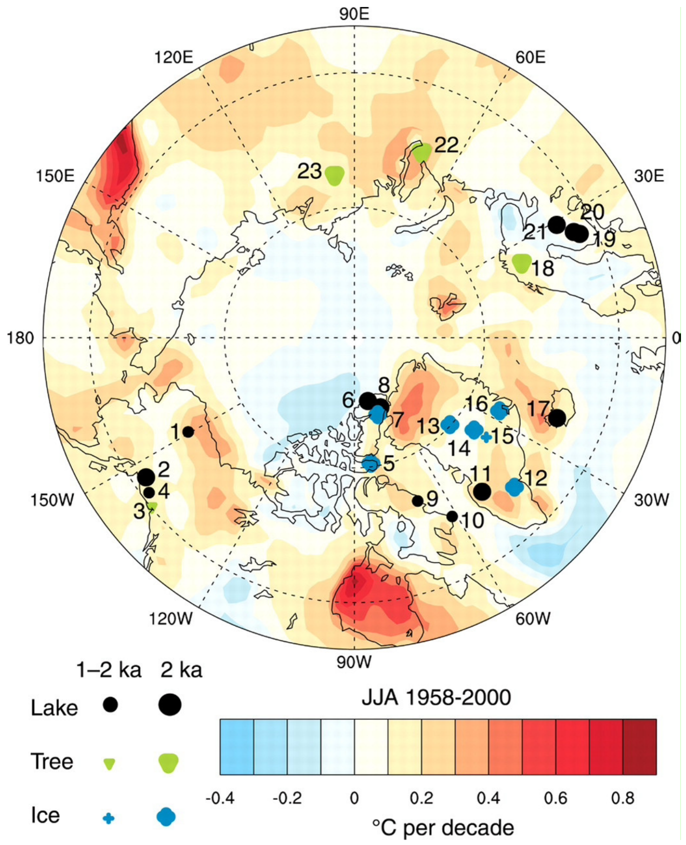

Locations of the proxy climate records included in the synthesis. Map colors indicate trends in summer (JJA) temperature between 1958 and 2000 from the ERA-40 data series. Large and small symbols indicate records that extend back to 2000 years ago (2 ka) and to at least 1000 years ago, respectively.

Kaufman et al. 2009. Recent Warming Reverses Long-Term Arctic Cooling. Science (80-.). 325, 1236–1239. https://doi.org/10.1126/science.1173983

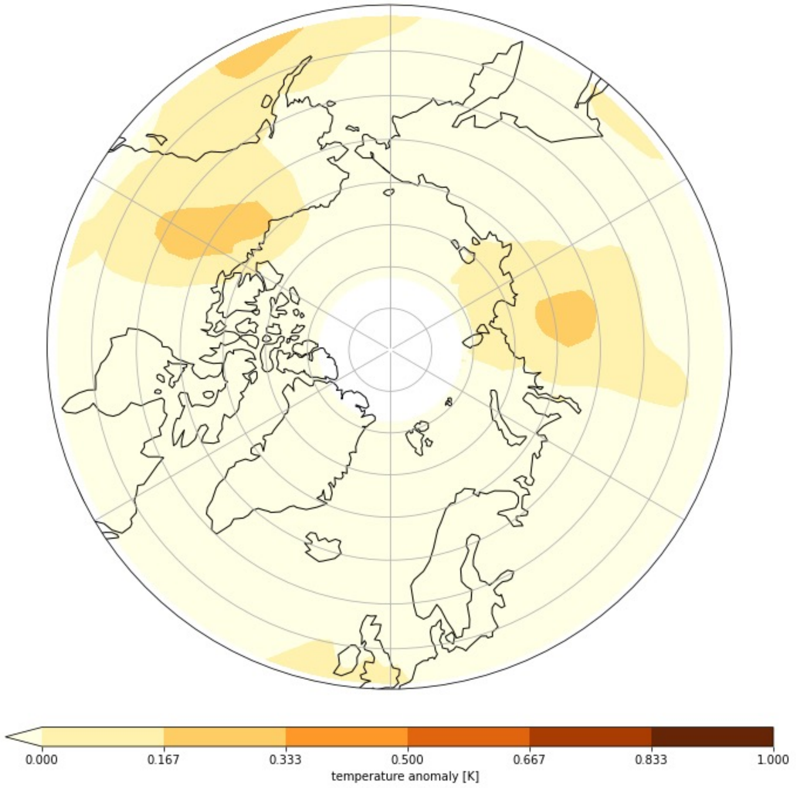

August UAH MSU lower troposphere before 2000

Emergence of the apparent Amplification (after 2000)

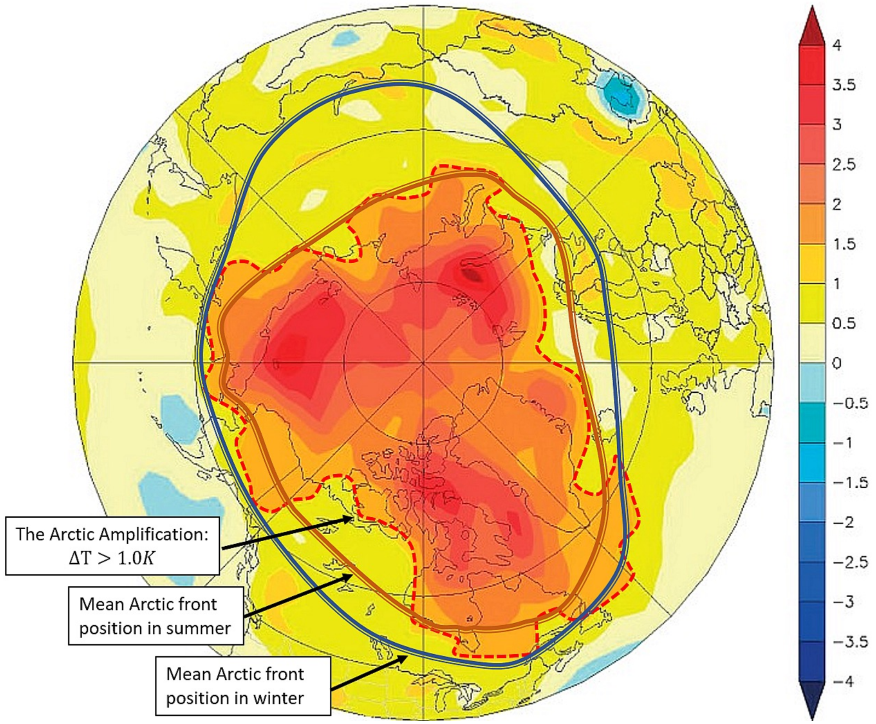

SAT after 2000

Annual UAH MSU lower troposphere after 2000

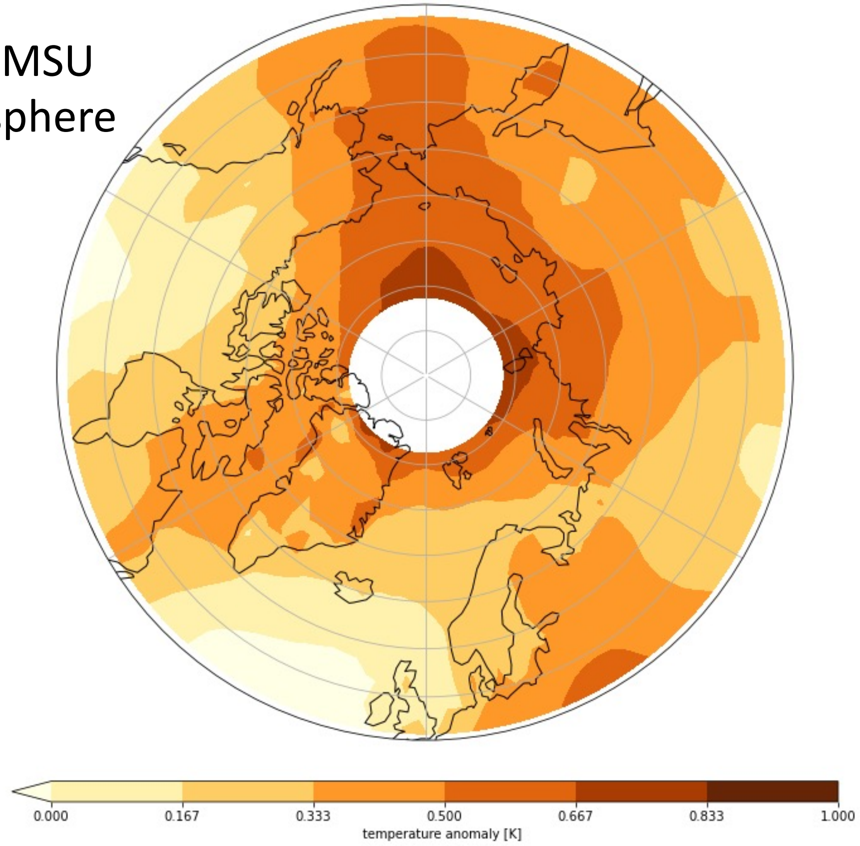

Geographical extents of the Amplification. The color shading represents the difference, ΔT, of **recent (2001-2012) annual averaged temperatures from a baseline period of 1971–2000** (Overland et al., 2014). Data are from NCEP/NCAR reanalysis. The Amplification core area is shown as the region of the temperature differences $\Delta T > 1.0\ K$ (dashed red line). The Arctic fronts are shown for the summer (brown line) and winter (blue line) seasons (Ladd and Gajewski, 2010).

The Amplification: observations and models after 2000

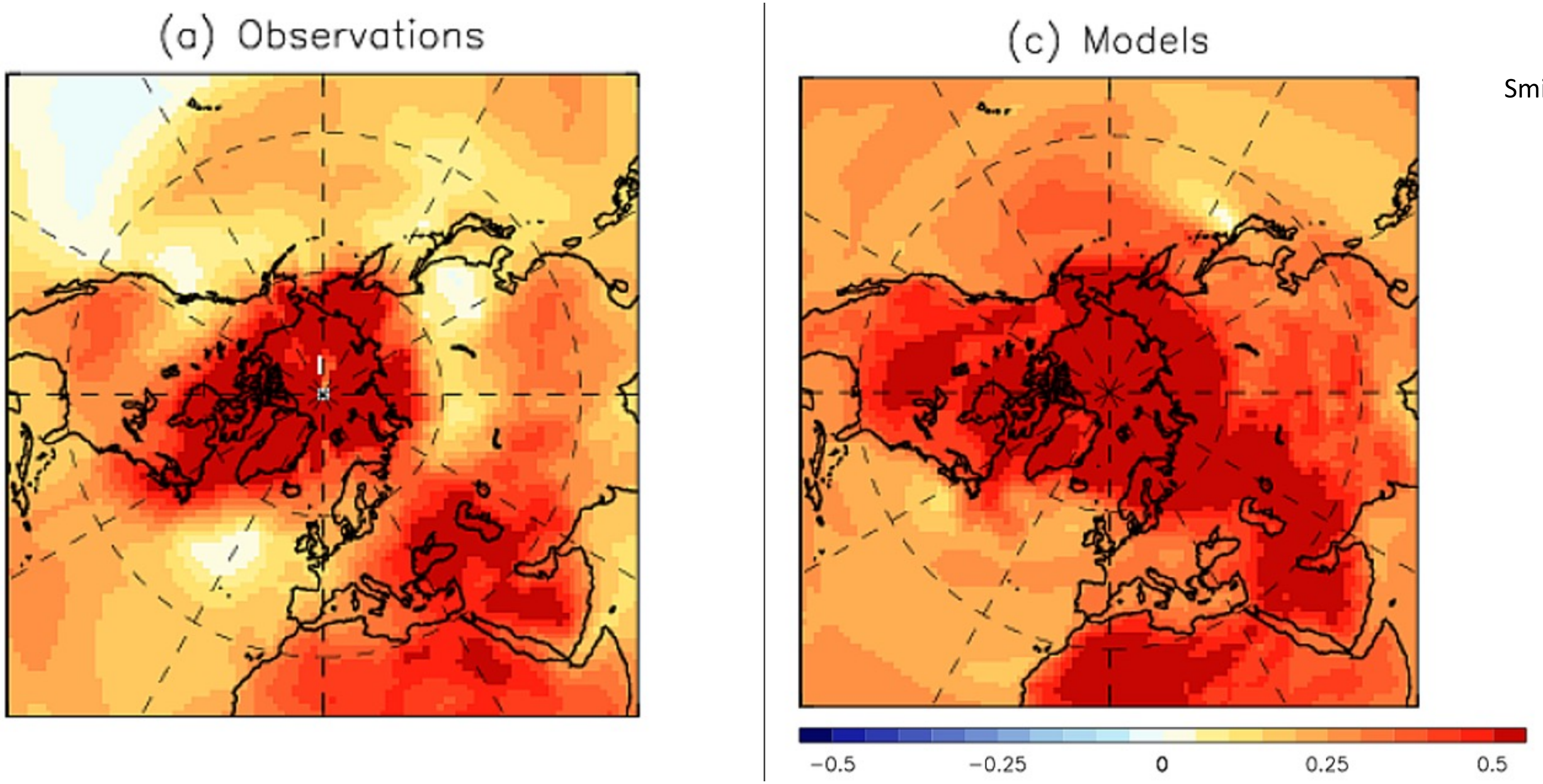

Smith, D. M., Screen, J. A., Deser, C., Cohen, J., Fyfe, J. C., García-Serrano, J., … Zhang, X. (2019). The Polar Amplification Model Intercomparison Project (PAMIP) contribution to CMIP6: investigating the causes and consequences of polar amplification. *Geoscientific Model Development*, *12*(3), 1139–1164. https://doi.org/10.5194/gmd-12-1139-2019

The Amplification represented by the temperature trends (^{o}C per decade for the 30-year period 1988-2017) in observations (a) and models (c). Observations are taken as the average of HadCRUT4 (Morice et al., 2012), NASA-GISS (Hansen et al., 2010) and NCDC (Karl et al., 2015). Model trends are computed as the average from 25 CMIP5 model simulations driven by historical and RCP4.5 radiative forcings. Source: (Smith et al., 2019b)

What has happened in early 2000s?

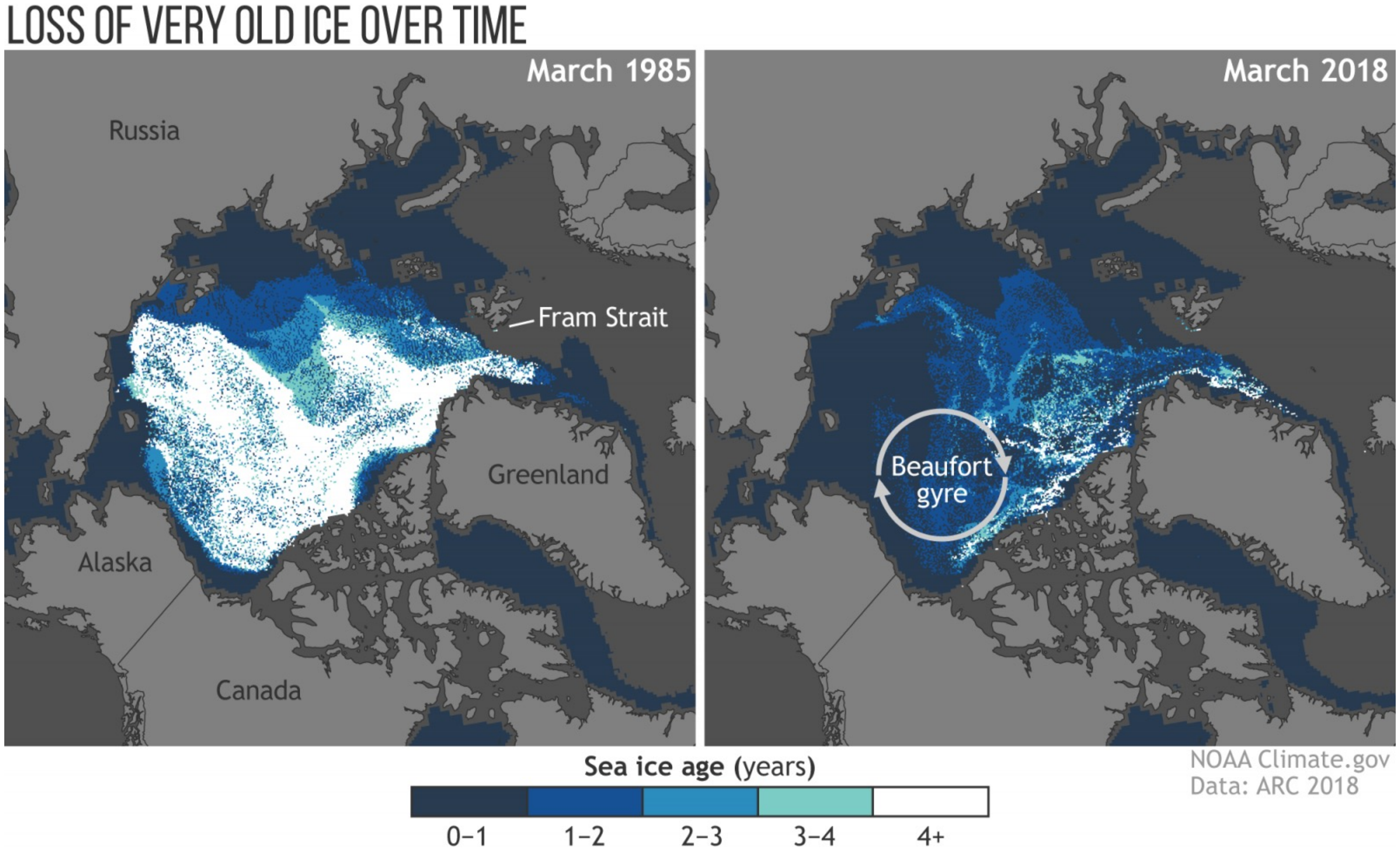

https://nsidc.org/cryosphere/seaice/characteristics/multiyear.html

In March 1985, sea ice that had survived at least four summers comprised **33%** of the Arctic ice pack at the winter maximum. In March 2019, such long-lasting sea ice comprised just over **1%**.
—Credit: NOAA Climate.gov, based on the Arctic Report Card: Update for 2019

Sea ice transitions

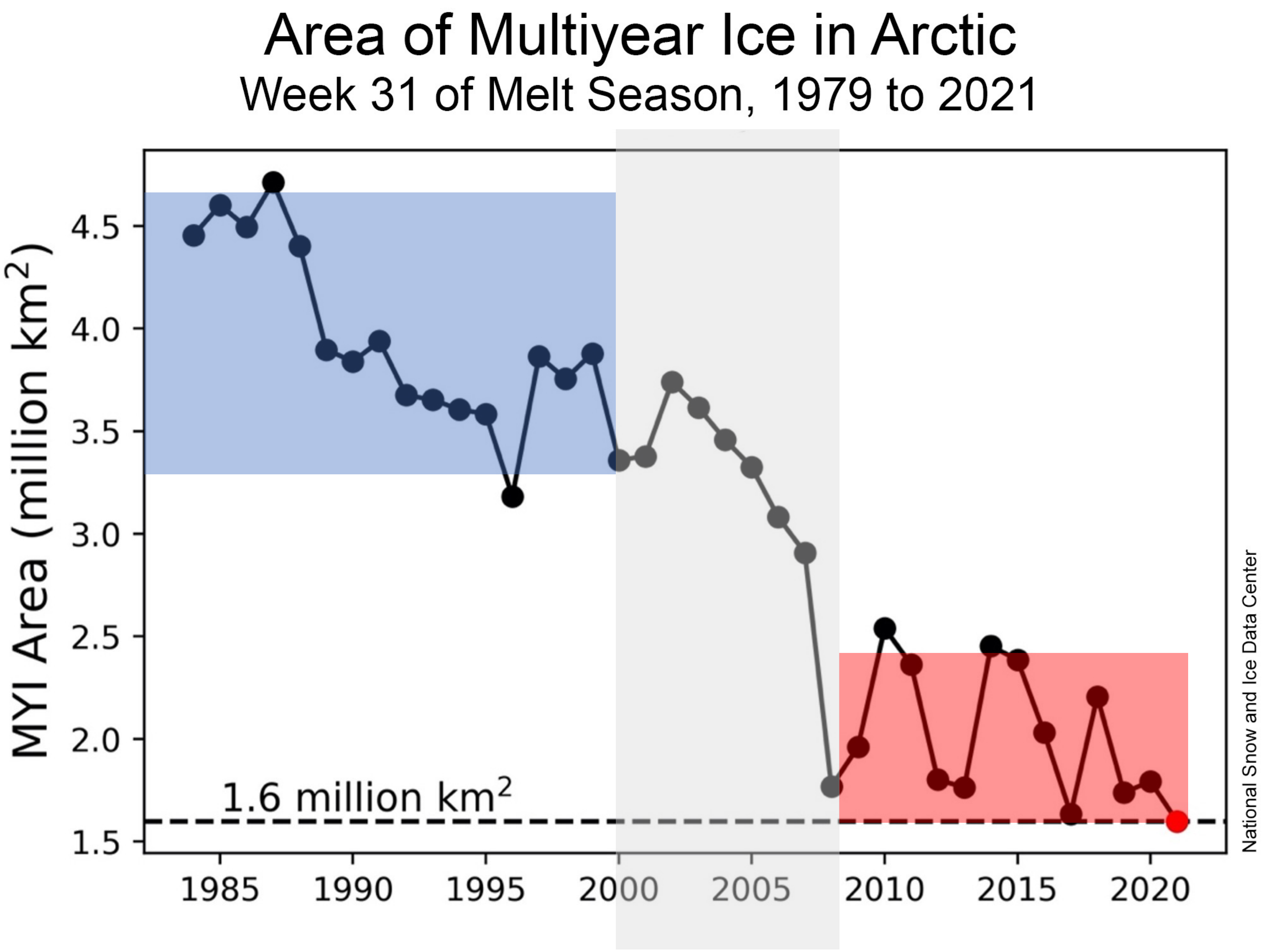

Liu, Y., Key, J.R., Wang, X., Tschudi, M., 2020. Multidecadal Arctic sea ice thickness and volume derived from ice age. Cryosph. 14, 1325–1345. https://doi.org/10.5194/tc-14-1325-2020

Sea ice transitions

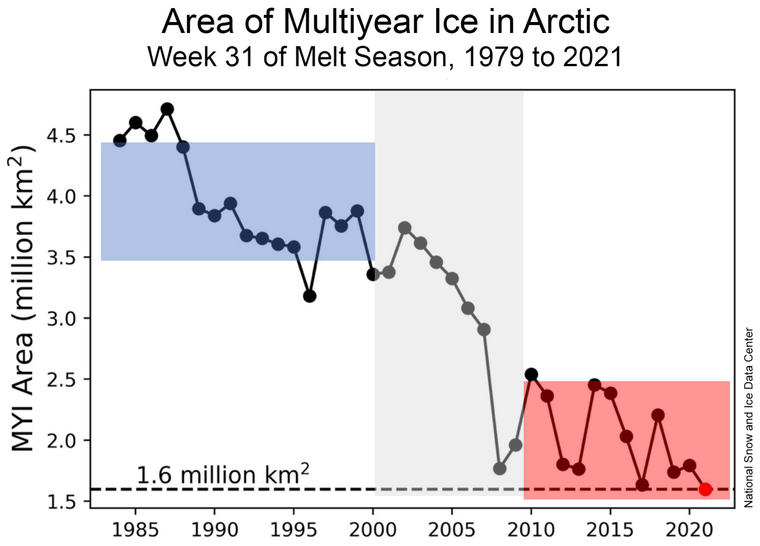

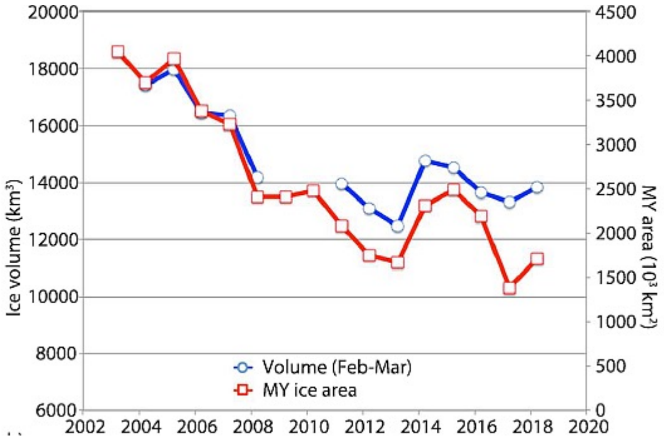

Kwok, R., 2018. Arctic sea ice thickness, volume, and multiyear ice coverage: Losses and coupled variability (1958-2018). Environ. Res. Lett. 13, 105005. https://doi.org/10.1088/1748-9326/aae3ec

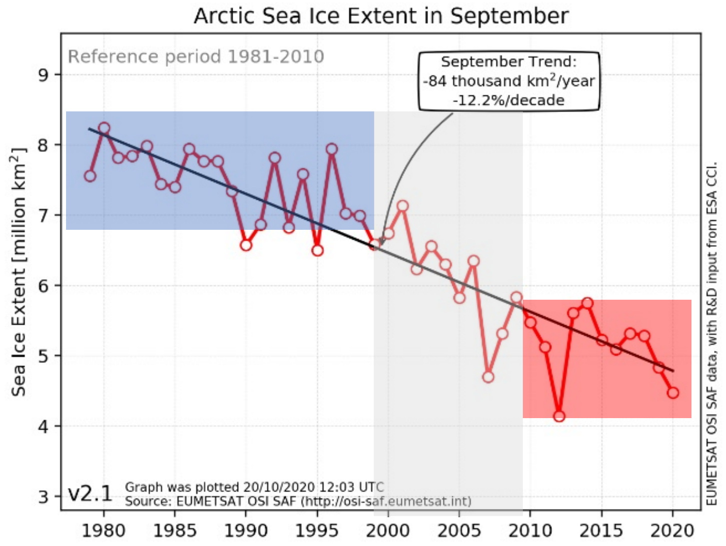

Liu, Y., Key, J.R., Wang, X., Tschudi, M., 2020. Multidecadal Arctic sea ice thickness and volume derived from ice age. Cryosph. 14, 1325–1345. https://doi.org/10.5194/tc-14-1325-2020

The Amplification and Sea Ice

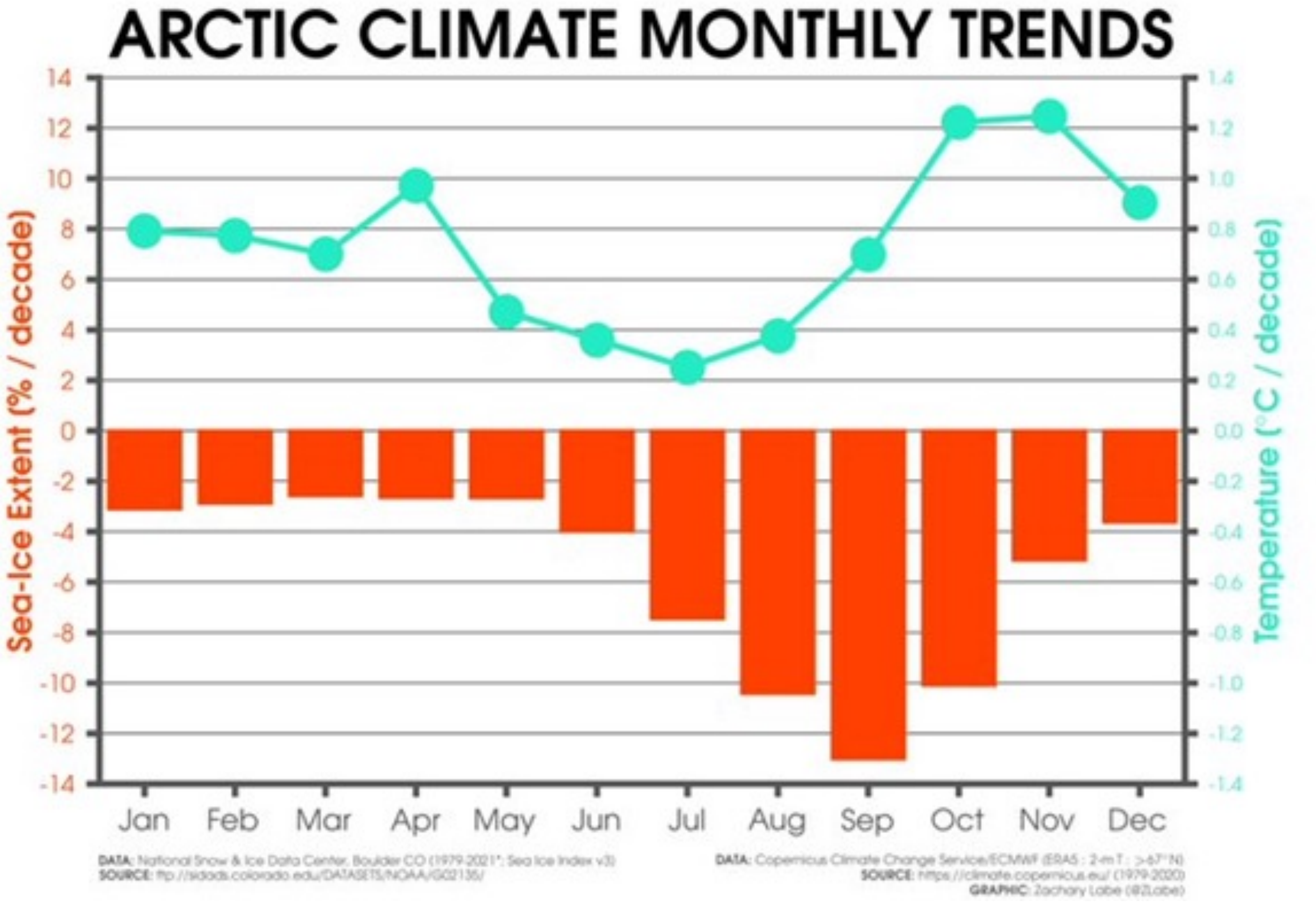

Seasonal trends in the sea ice extent (% dec-1) and the surface air temperature (oC dec-1) in the Arctic Ocean domain. Courtesy: Zack Labe.

Emergence of the *apparent* Amplification in satellite data

Courtesy: Esau et al.

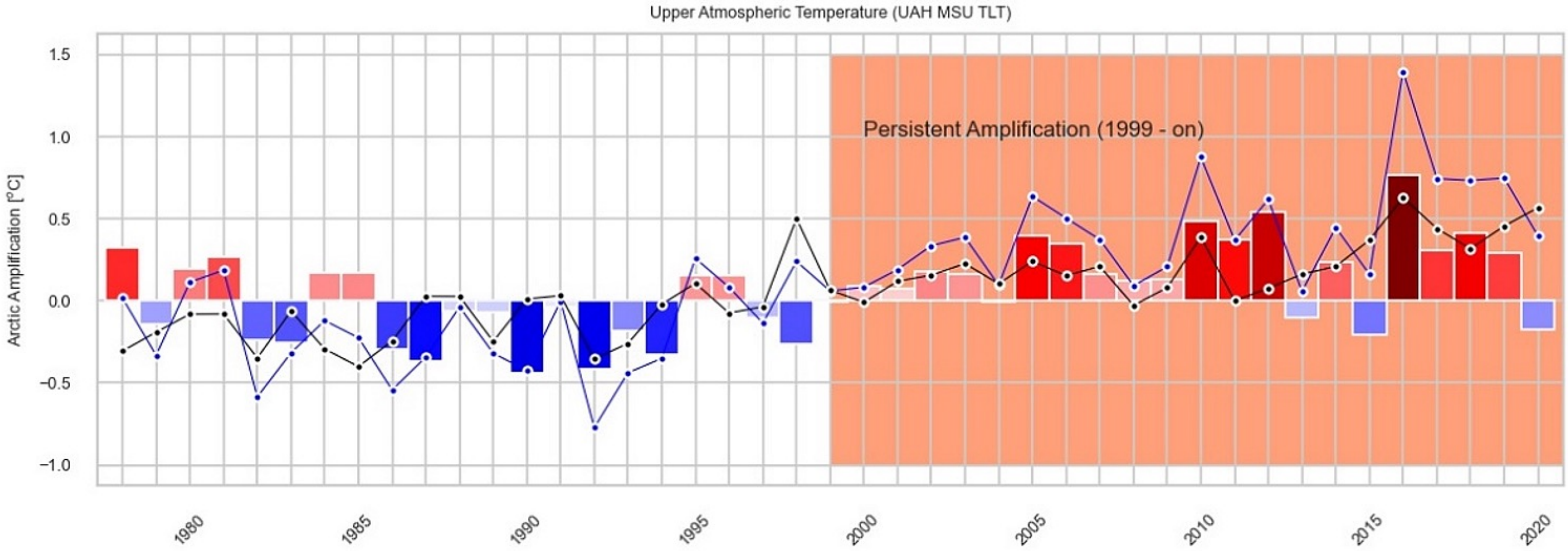

Shrubification of tundra

Emergence of global warming

Period of hidden Amplification

Period of apparent Amplification

Period of saturated Amplification

Sea ice transition (strong reduction of multiyear ice)

Cloud co-variability

Jun, S.-Y., Ho, C.-H., Jeong, J.-H., Choi, Y.-S., & Kim, B.-M. (2016). Recent changes in winter Arctic clouds and their relationships with sea ice and atmospheric conditions. *Tellus A: Dynamic Meteorology and Oceanography*, *68*(1), 29130. https://doi.org/10.3402/tellusa.v68.29130

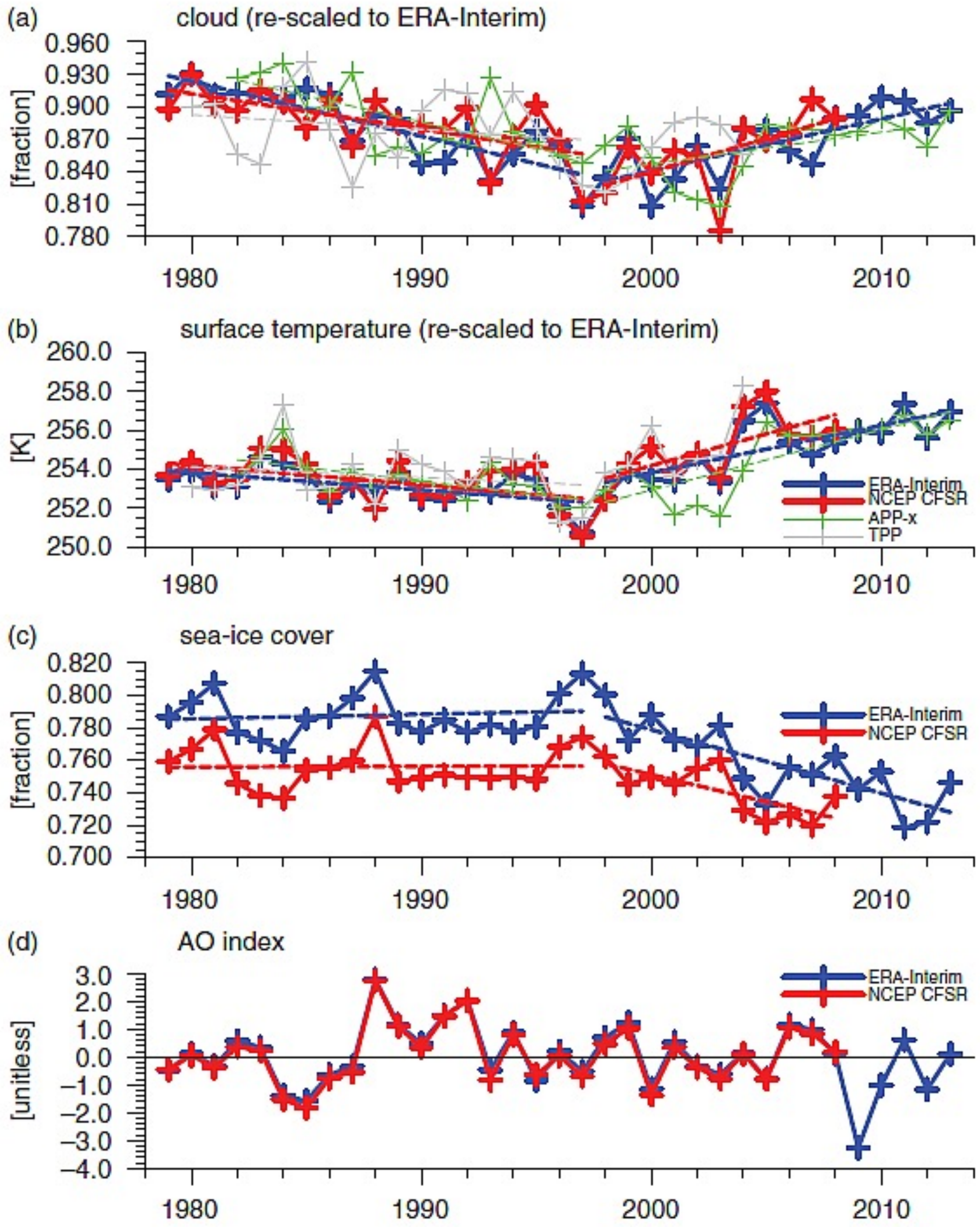

Time series of (a) cloud amount, (b) surface temperature, (c) sea ice cover over the Arctic Ocean (north of 678N) and (d) Arctic Oscillation (AO) index in winter (December through February) from ERA-Interim, NCEP CFSR, APP-x and TPP datasets. Long-term trends are denoted with dashed lines. The time series of cloud amount, surface temperature and sea ice cover are re-scaled to adopt the mean and standard deviation of ERAInterim for comparison.

Courtesy: Esau et al.

Cloud-related feedbacks

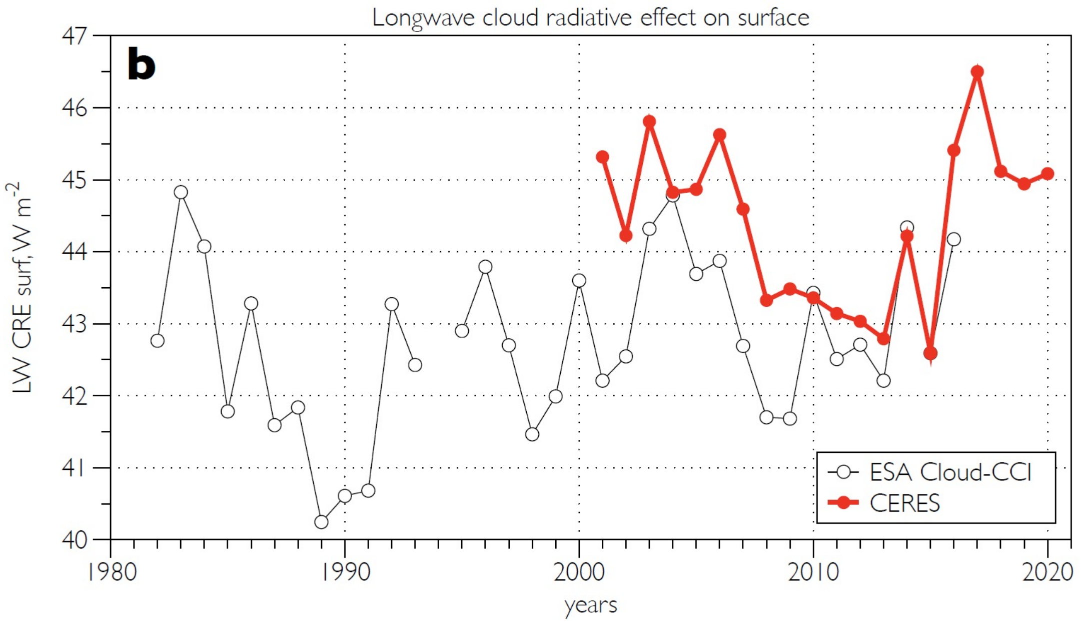

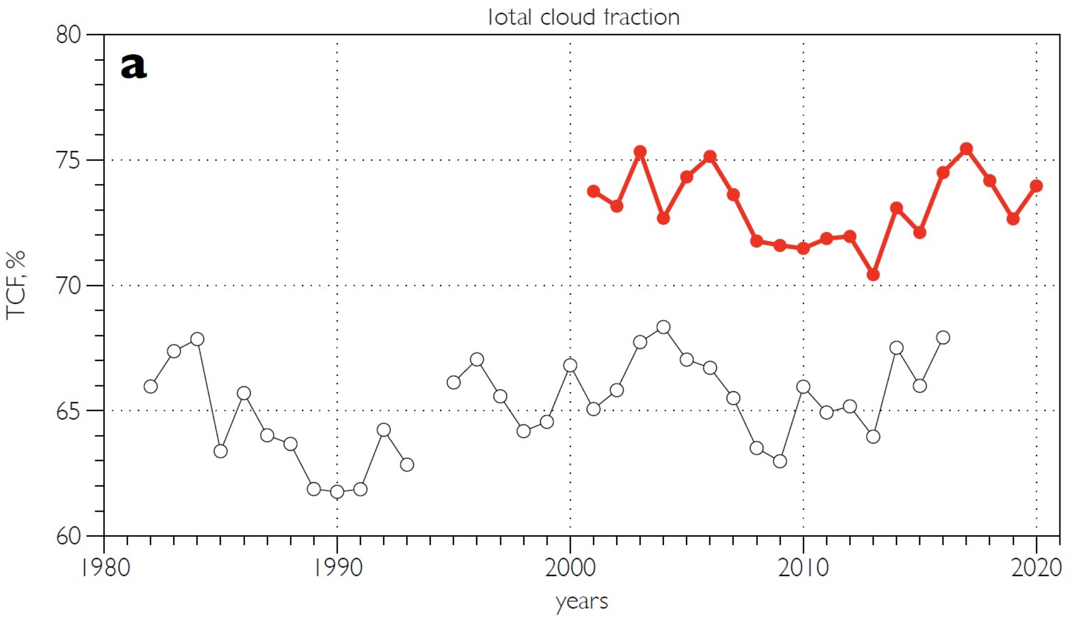

Impact of the Amplification

Afforestation of a burned tundra area in the northern West Siberia. The left image is taken by Corona/KH-4b, 21.08.1968; the right image – by Resurs-P, 28.09.2016. Source: (Sizov et al., 2020).

Vegetation height

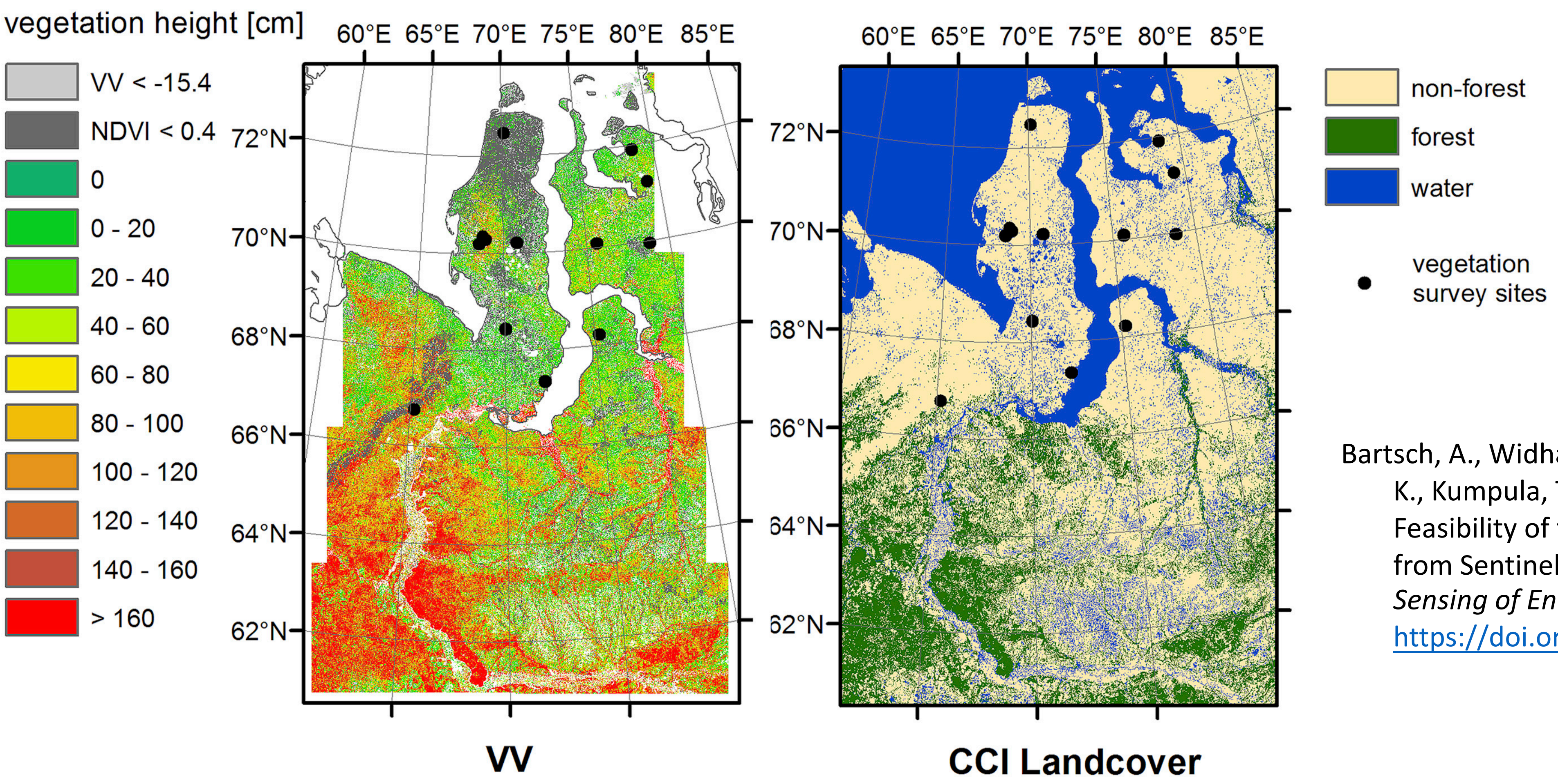

Bartsch, A., Widhalm, B., Leibman, M., Ermokhina, K., Kumpula, T., Skarin, A., … Pointner, G. (2020). Feasibility of tundra vegetation height retrieval from Sentinel-1 and Sentinel-2 data. *Remote Sensing of Environment*, *237*. https://doi.org/10.1016/j.rse.2019.111515

Shrubification

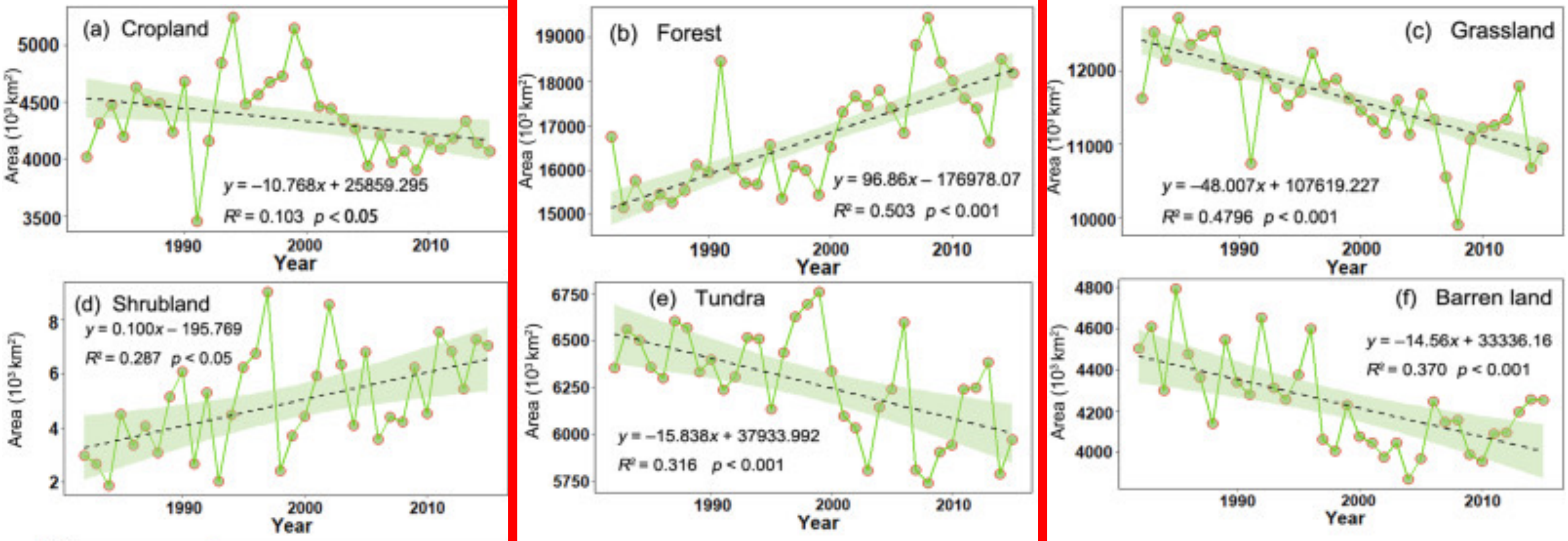

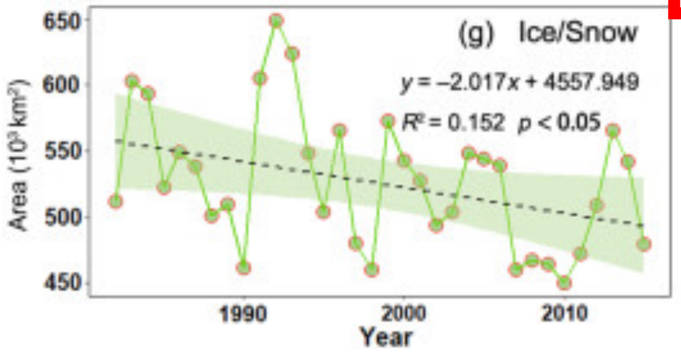

Changing trends in NDVI values from 1982 to 2015 for different land cover types using robust linear regressions (The NDVI values were the maximum values in each year).

The NDVI data were calculated using the third-generation dataset from the Global Inventory Modeling and Mapping Studies (GIMMS) The land cover types data were obtained from the annual dynamics of global land cover (GLASS-GLC) published in 2020

Xue, S.-Y., Xu, H.-Y., Mu, C.-C., Wu, T.-H., Li, W.-P., Zhang, W.-X., Streletskaya, I., Grebenets, V., Sokratov, S., Kizyakov, A., Wu, X.-D., 2021. Changes in different land cover areas and NDVI values in northern latitudes from 1982 to 2015. Adv. Clim. Chang. Res. https://doi.org/10.1016/j.accre.2021.04.003

Surface morphology changes

Nitze, I., Grosse, G., Jones, B. M., Romanovsky, V. E., & Boike, J. (2018). Remote sensing quantifies widespread abundance of permafrost region disturbances across the Arctic and Subarctic. *Nature Communications*, *9*(1), 1–11. https://doi.org/10.1038/s41467-018-07663-3

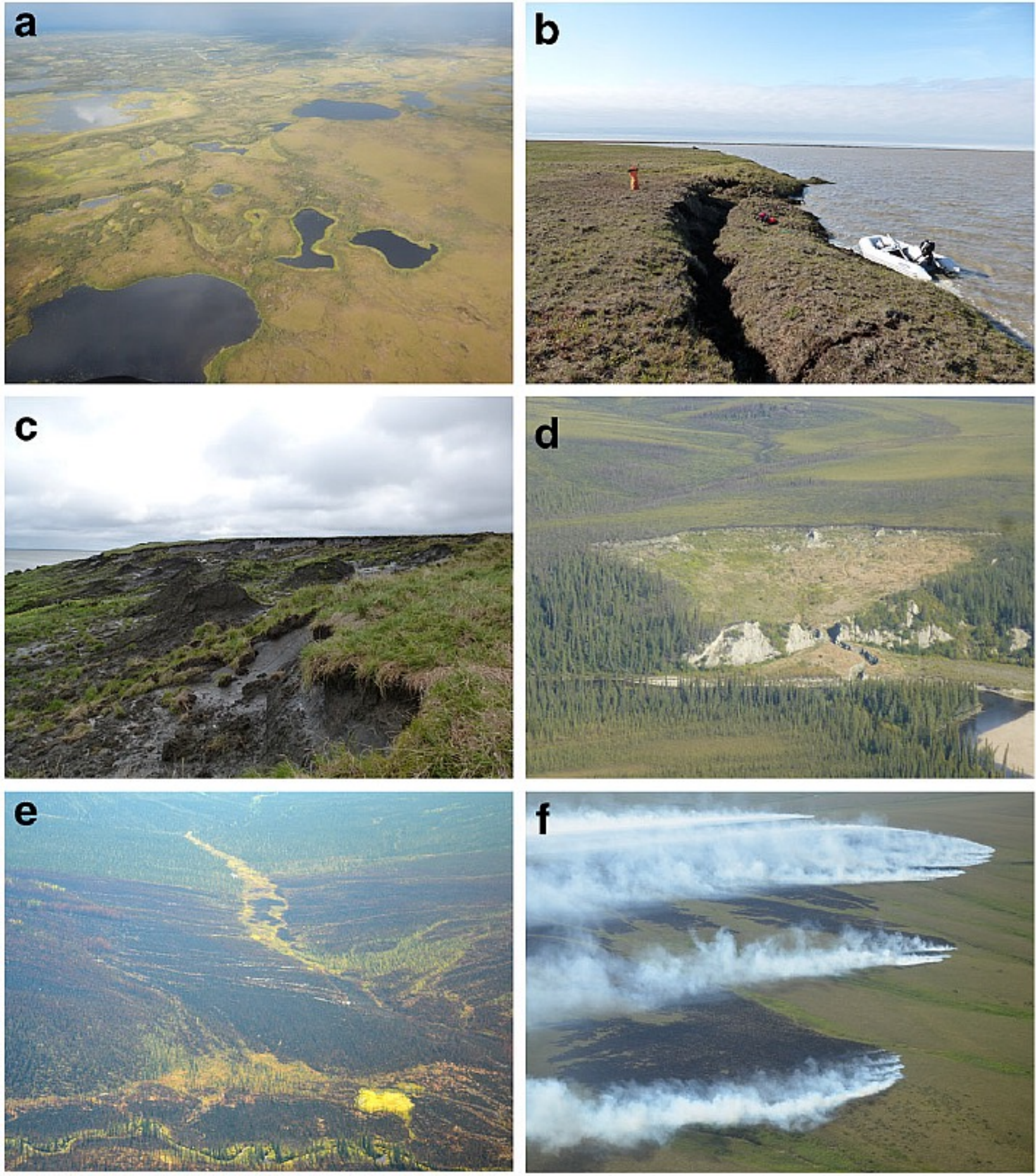

Examples of key permafrost region disturbances. a Dynamic lake-rich region in western Alaska with frequent drainage, b Expanding thermokarst lake in northern Alaska, c Coastal retrogressive thaw slump on Bykovsky Peninsula in northeastern Siberia, d Selawik thaw slump in western Alaska, e Burn scar of wildfire in boreal Alaska, and f Burning tundra fire in northern Alaska. Photos taken by I. Nitze (b−d), B.M. Jones (e, f), and M. Fuchs (a)

Permafrost (example of a morphological method)

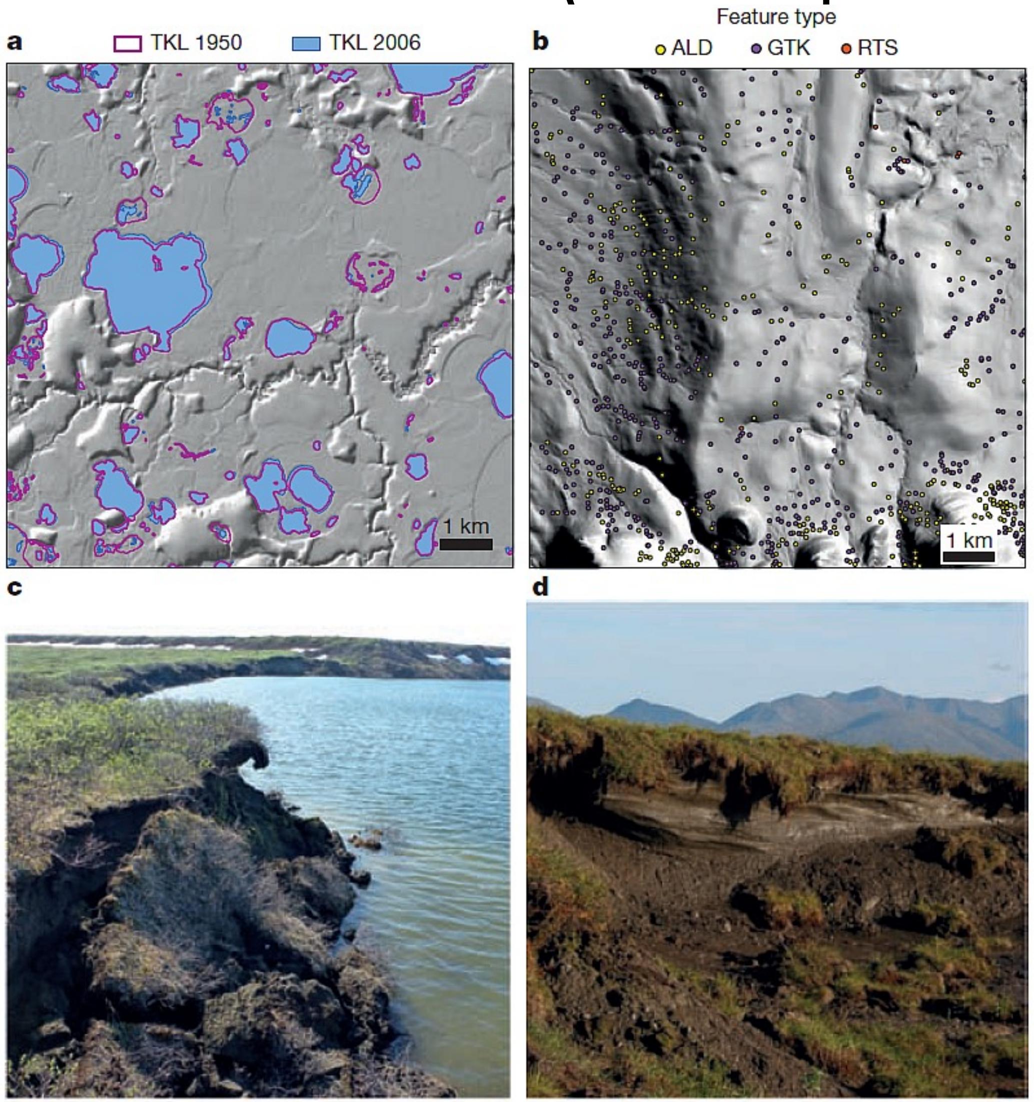

Abundance of abrupt thaw features in lowland and upland settings in Alaska. Left panels (a, c) show thermokarst lake (TKL) abundance, expansion, and drainage on the Seward Peninsula, Northwest Alaska, between 1950 and 2006, with collapsing permafrost banks. Right panels (b, d) show extensive distribution of ground collapse and erosion features (ALD, active layer detachment slide; RTS, retrogressive thaw slump; GTK, thermal erosion gullies) in upland tundra in a hill slope region in Northwest Alaska and thawing icy soils in a retrogressive thaw slump.

Schuur, E. A. G., McGuire, A. D., Schädel, C., Grosse, G., Harden, J. W., Hayes, D. J., … Vonk, J. E. (2015). Climate change and the permafrost carbon feedback. *Nature*, *520*(7546), 171–179. https://doi.org/10.1038/nature14338

Sea ice impact on primary production

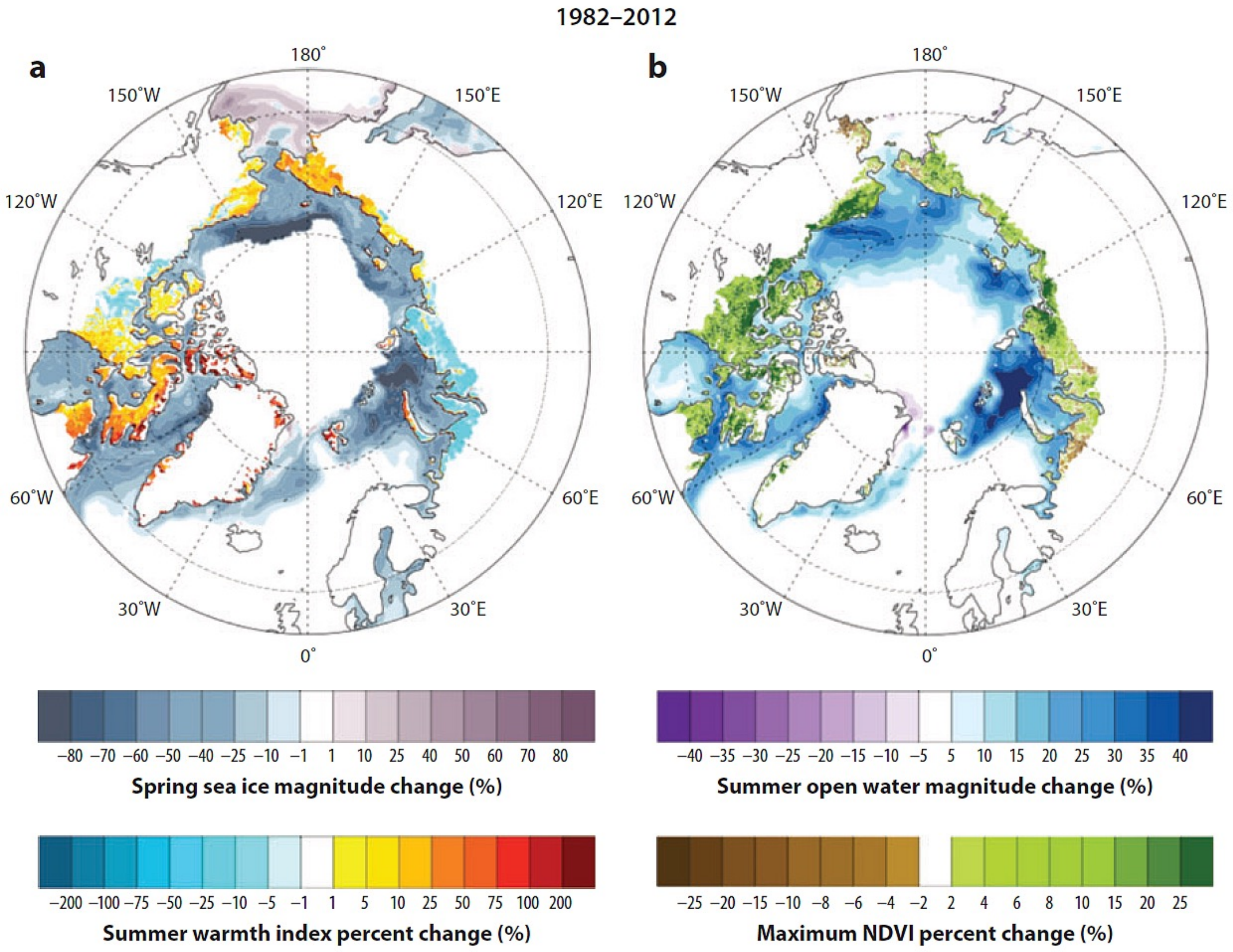

Percent trends (1982–2012) for (*a*) spring sea ice concentration (%) (as represented by trends from the climatological 50% sea ice concentration level) and land-surface summer warmth index (◦C month), (*b*) summer (May–August) open water area (%) and annual maximum NDVI (Normalized Difference Vegetation Index; unitless). The percent trend highlights the size of relative changes in the Arctic.

Bhatt, U.S., Walker, D.A., Walsh, J.E., Carmack, E.C., Frey, K.E., Meier, W.N., Moore, S.E., Parmentier, F.-J.W., Post, E., Romanovsky, V.E., Simpson, W.R., 2014. Implications of Arctic Sea Ice Decline for the Earth System. Annu. Rev. Environ. Resour. 39, 57–89. https://doi.org/10.1146/annurev-environ-122012-094357

Key studies (1)

Reference	Brief description
Box et al., 2019. Key indicators of Arctic climate change: 1971-2017. Environ. Res. Lett. 14, 45010. https://doi.org/10.1088/1748-9326/aafc1b	Overview of **the Arctic climate change**
Previdi et al, 2021. Arctic amplification of climate change: A review of underlying mechanisms. Environ. Res. Lett. 16. https://doi.org/10.1088/1748-9326/ac1c29	Comprehensive and systematic review of the Amplification, primarily based on **modeling** studies
Mayer et al., 2019. An Improved Estimate of the Coupled Arctic Energy Budget. J. Clim. 32, 7915–7934. https://doi.org/10.1175/JCLI-D-19-0233.1	The Arctic **energy budget**
Yang et al., 2013. The role of satellite remote sensing in climate change studies. Nat. Clim. Chang. 3, 875–883. https://doi.org/10.1038/nclimate1908	Contribution of the **satellite observations in the climate change** science
Duncan et al., 2020. Space-Based Observations for Understanding Changes in the Arctic-Boreal Zone. Rev. Geophys. 58, 1–95. https://doi.org/10.1029/2019RG000652	Comprehensive review of **satellite observations** in the Arctic climate science
Plummer et al., 2017. The ESA Climate Change Initiative (CCI): A European contribution to the generation of the Global Climate Observing System. Remote Sens. Environ. 203, 2–8. https://doi.org/10.1016/j.rse.2017.07.014	Overview of the **ESA CCI** for climate studies
Jenkins et al., 2020. Satellite-based decadal change assessments of pan-Arctic environments. Ambio, 49(3), 820–832.	Satellite observations in the **environmental assessment**
Devasthale et al., 2020. A Climatological Overview of Arctic Clouds. pp. 331–360. https://doi.org/10.1007/978-3-030-33566-3_5 Stengel et al., 2020. Cloud CCI : 35-year climatology of global cloud and radiation properties. Earth Syst. Sci. Data 12, 41–60. https://doi.org/10.5194/essd-12-41-2020	Satellite observations of the **Arctic clouds**

Key studies (2)

Reference	Brief description
Liu et al., 2020. Multidecadal Arctic sea ice thickness and volume derived from ice age. Cryosphere 14, 1325–1345. https://doi.org/10.5194/tc-14-1325-2020	**Sea ice** characteristics from satellites
Bormann et al., 2018. Estimating snow-cover trends from space. Nat. Clim. Chang. 8, 924–928. https://doi.org/10.1038/s41558-018-0318-3	**Snow cover** characteristics from satellites

The Amplification Drivers

Driver	Trend	Effect
TOA radiation balance	More negative (-0.19 ± 0.44 W m^{-2} K^{-1})	Insignificant
Surface radiation balance	Less negative	Enhancing: - Positive ice-albedo and heat storage feedbacks
Clouds	Uncertain – data disagree Low-level clouds likely increasing	Enhancing: - Positive LW radiation feedback
Atmospheric humidity	Increasing	Enhancing
Sea ice cover and volume	Strongly decreasing	Enhancing: - Positive albedo feedback - Positive LW radiation feedback
CO2 increase	Strongly increasing	Enhancing: - More positive LW radiation feedback in cold areas

Impact of the Amplification

Sizov et al., 2020. Assessment of the post-pyrogenic dynamics of tundra vegetation in the northern part of Western Siberia over the past 50 years (1968–2018) based on detailed and high resolution remote sensing data. Sovrem. Probl. distantsionnogo Zo. Zemli iz kosmosa 17, 137–153. https://doi.org/10.21046/2070-7401-2020-17-4-137-153